Earth and Planetary Science Letters 454 (2016) 1–9

Contents lists available at ScienceDirect

Earth and Planetary Science Letters

www.elsevier.com/locate/epsl

In situ measurement of atmospheric krypton and xenon on Mars with Mars Science Laboratory

P.G. Conrad [a,*], C.A. Malespin [a,b], H.B. Franz [a,c], R.O. Pepin [d], M.G. Trainer [a], S.P. Schwenzer [e], S.K. Atreya [f], C. Freissinet [a], J.H. Jones [g], H. Manning [h], T. Owen [i], A.A. Pavlov [a], R.C. Wiens [j], M.H. Wong [f], P.R. Mahaffy [a]

[a] Solar System Exploration Division, NASA Goddard Space Flight Center, Greenbelt, MD 20771, USA
[b] Universities Space Research Association (USRA), Columbia, MD, USA
[c] CRESST, UMBC, NASA GSFC, Greenbelt, MD 20771, USA
[d] University of Minnesota, Minneapolis, MN 55455, USA
[e] The Open University, Department for Environment, Earth and Ecosystems, Walton Hall, Milton Keynes MK6 3AQ, United Kingdom
[f] Climate and Space Sciences and Engineering, University of Michigan, Ann Arbor, MI 48109-2143, USA
[g] XI-3, ARES, NASA/JSC, Houston, TX 77058, USA
[h] Concordia University, Moorhead, MN 56562, USA
[i] University of Hawaii, Honolulu, HI 96822, USA
[j] Los Alamos National Laboratory, Los Alamos, NM 87545, USA

ARTICLE INFO

Article history:
Received 26 March 2016
Received in revised form 12 August 2016
Accepted 17 August 2016
Available online xxxx
Editor: B. Marty

Keywords:
krypton
xenon
Mars atmosphere
Mars evolution
Mars Science Laboratory
Mars meteorites

ABSTRACT

Mars Science Laboratory's Sample Analysis at Mars (SAM) investigation has measured all of the stable isotopes of the heavy noble gases krypton and xenon in the martian atmosphere, *in situ*, from the Curiosity Rover at Gale Crater, Mars. Previous knowledge of martian atmospheric krypton and xenon isotope ratios has been based upon a combination of the Viking mission's krypton and xenon detections and measurements of noble gas isotope ratios in martian meteorites. However, the meteorite measurements reveal an impure mixture of atmospheric, mantle, and spallation contributions. The xenon and krypton isotopic measurements reported here include the complete set of stable isotopes, unmeasured by Viking. The new results generally agree with Mars meteorite measurements but also provide a unique opportunity to identify various non-atmospheric heavy noble gas components in the meteorites. Kr isotopic measurements define a solar-like atmospheric composition, but deviating from the solar wind pattern at ^{80}Kr and ^{82}Kr in a manner consistent with contributions originating from neutron capture in Br. The Xe measurements suggest an intriguing possibility that isotopes lighter than ^{132}Xe have been enriched to varying degrees by spallation and neutron capture products degassed to the atmosphere from the regolith, and a model is constructed to explore this possibility. Such a spallation component, however, is not apparent in atmospheric Xe trapped in the glassy phases of martian meteorites.

Published by Elsevier B.V.

1. Introduction

The noble gases are key indicators of planetary evolution. Krypton and xenon are especially useful with their large numbers of stable isotopes; six and nine respectively, making them ideal for tracking source reservoirs and for understanding the evolution of planetary interiors and atmospheres. Many of the isotopes are formed or fractionated by distinct mechanisms, so their enrichment or depletion can be informative with regard to source: ^{129}Xe is produced by decay of ^{129}I, a now extinct radioactive nuclide with a half-life of 15.7 Myr. Isotopes ^{131}Xe, ^{132}Xe, ^{134}Xe and ^{136}Xe are produced by actinide fission. Radiogenic ^{129}Xe and ^{136}Xe can be used (along with other noble gas isotopes) to test hypotheses for atmospheric formation and loss: their ^{129}I and ^{244}Pu parent species abundances at the time of Earth and Mars' formation are constrained by their radiogenic daughters in the atmospheres. Comparison of planetary interior values (trapped in mantle phases of igneous rocks) with atmospheric abundances and solar wind abundances can reveal how long ago ^{129}Xe and ^{136}Xe were degassed (Podosek and Ozima, 2000). Excess ^{129}Xe relative to ^{130}Xe in Mars' atmosphere relative to interior components supports the hypothesis that Mars degassed soon after planetary

* Corresponding author.
E-mail address: Pamela.G.Conrad@nasa.gov (P.G. Conrad).

http://dx.doi.org/10.1016/j.epsl.2016.08.028
0012-821X/Published by Elsevier B.V.

accretion, while fractionation of Xe isotopes in the martian atmosphere may indicate substantial loss of atmosphere in a very early hydrodynamic escape phase (Pepin, 1991, 2000).

Previous to MSL, what we knew about martian noble gases was based on the noble gas measurements of Viking (Owen and Biemann, 1976; Owen et al., 1976, 1977) and the analyses of meteorites ejected from Mars. These meteorites: shergottites (Treiman and Filiberto, 2015), nakhlites (Treiman, 2005), chassignites (Treiman et al., 2007), ALH84001 (Treiman, 1998) and the basaltic breccia NWA7034 (Agee et al., 2013) are petrologically distinct from primitive chondritic meteorites, and the compositional similarity of gases trapped in their impact melt inclusions to Mars' atmospheric values is what identified them as martian (Bogard and Johnson, 1983; Pepin, 1985; Wiens and Pepin, 1988). But martian meteorites all contain more than one noble gas component, and measurements therefore return a composite of unfractionated or fractionated martian atmosphere, martian interior gases, fission and cosmogenic additions, and terrestrial contamination.

An elementally unfractionated martian atmospheric component was first found in shock melt inclusions in the shergottite EETA 79001 (Bogard and Johnson, 1983; Becker and Pepin, 1984; Wiens et al., 1986; Swindle et al., 1986), establishing the link between the SNC meteorites and Mars. The Xe composition was found to be isotopically distinct from all other known xenon reservoirs, especially in its high $^{129}Xe/^{132}Xe$ ratio and enhanced $^{134}Xe/^{132}Xe$ and $^{136}Xe/^{132}Xe$ ratios (Swindle et al., 1986). This atmospheric component was refined using a range of shock melts from four different shergottites, resulting in a recommended $^{129}Xe/^{132}Xe$ ratio of 2.60 ± 0.05 for Mars' atmosphere (Bogard and Garrison, 1998). Most recently, a martian brecciated meteorite (NWA7034, 'Black Beauty') (Agee et al., 2013) was shown to contain dominantly unfractionated martian atmosphere (Cartwright et al., 2014), providing evidence that this component is not unique to the shergottites. Elementally fractionated Martian atmospheric component(s) are found in the nakhlites and ALH84001 (Swindle, 2002) and the Martian interior component was first identified in the Chassigny meteorite (Ott, 1988).

Terrestrial air can introduce both unfractionated and fractionated contamination to meteorites, with the latter mimicking interior signals (Mohapatra et al., 2009) or completely masking martian signatures (Schwenzer et al., 2013). Disentangling those components is key to understanding processes such as planetary formation. It also provides insights into surface–atmosphere interaction and ejection history, but only at the precision with which the individual components are known and understood. Precise *in situ* measurements of Xe and Kr in Mars' atmosphere are not hampered by complications introduced by "contaminating" noble gases.

2. Experimental

Previously, we reported measurements of the stable isotopes of argon: $^{40}Ar/^{36}Ar = 1.9 \pm 0.3 \times 10^3$ and $^{36}Ar/^{38}Ar = 4.2 \pm 0.1$ (Atreya et al., 2013; Mahaffy et al., 2013). The $^{40}Ar/^{36}Ar$ ratio used dynamic mass spectrometry to directly measure these masses. To obtain the ratio of ^{36}Ar to ^{38}Ar, it was necessary to develop a semi-static enrichment experiment to reach sufficiently high signal-to-noise (S/N) and background contrast for measurement of ^{38}Ar, the least-abundant Ar isotope (Atreya et al., 2013). However, while semi-static experiments provided moderate S/N and low enough background contrast to also enable Kr isotope measurements, they were unable to enrich the Xe signals to the extent necessary for precise isotopic measurement. That required development of a fully static mass spectrometry experiment (Table 1).

Table 1
Semi-static and static SAM experiments on Mars.

Experiment ID	Solar longitude	Sol
Semi-static enrichment mass spectrometry		
25111 (Kr)	358	341
25269 (Kr)	336	976
Static mass spectrometry		
25253 (Xe)	301	915
25269 (Xe)	336	976

2.1. Static mass spectrometry

The relevant components of the SAM suite are described in Mahaffy et al. (2012). Gas is ingested, flowing through both zeolite (Linde 13x) and magnesium sulfate chemical scrubbers, effectively removing >95% of the CO_2 and H_2O, and weakly adsorbing all other active gases. The post-scrubber gas mix is enriched in N_2, Ar, Kr, and Xe, which then flows over a cooled hydrocarbon (HC) trap to efficiently trap out Xe, allowing other gases to pass. The HC trap consists of three adsorbents in series, Tenax® TA, silica beads, and carbosieve®. The approach and scripting were validated in the SAM high fidelity test bed at Goddard Space Flight Center.

The tunable laser spectrometer (TLS), which has been evacuated prior to atmospheric ingestion, is used as a storage volume so that gases not trapped out on the HC trap, particularly Kr, are collected here for later analysis.

The enrichment flows gas over the scrubbers and trap for 5400 s, after which the HC trap and TLS are closed off from the rest of the SAM manifolds. The manifolds are evacuated, and the scrubbers activated to clean them of adsorbed gas.

Xe-enriched gas collected on the trap is slowly released into the quadrupole mass spectrometer (QMS) in a semi-static scanning mode, where the conductance out to the pump is throttled to increase the S/N in the MS. Once the majority of the gas has been released into the manifold, the valve to the pump is closed, and the remaining gas is scanned in fully static mode. The low abundance of Xe allows fully static mode without increasing the pressure inside the mass spectrometer to a saturated level. The masses of interest (the nine stable Xe isotopes) are scanned. Once analysis of Xe is complete, the manifolds and MS are evacuated prior to releasing the Kr-enriched gas from the TLS. The QMS is returned to semi-static mode for analysis of Kr; static mode being too risky because of the high Ar partial pressure in the gas. Because Kr and Xe cannot be scanned at the same time in this method a direct measurement of the $^{84}Kr/^{132}Xe$ elemental ratio could not be obtained, nor could $^{84}Kr/^{36}Ar$ since the enrichment of ^{36}Ar saturates the detector.

2.2. Data processing

Experimental Kr and Xe data were corrected for detector dead time, mass discrimination (Appendix A1), quadrupole mass spectrometer (QMS) tuning effects, and instrument background, as discussed in Franz et al. (2014). Because the background as well as analytic signal grew with time during the semi-static and static QMS modes utilized for Kr and Xe measurements, background models were based on tracer m/z representative of the instrument background. For Kr, a tracer of m/z 12 was used in experiment ID #25111 and m/z 79 in ID #25269. For Xe, m/z 127 was used as the tracer in both ID #25253 and ID #25269. The background model is implemented by scaling the trend exhibited by the tracer m/z based on the relative proportions of the analyte and tracer m/z during the background region prior to introduction of Xe or Kr gas to the manifold. Uncertainties in the background model were computed from the difference in isotope ratios derived with the

Table 2
Xenon.[a]

	124/132	126/132	128/132	129/132	130/132	131/132	134/132	136/132
ID#25253 (Static)	0.00483	0.00368	0.0757	2.5268	0.1542	0.8105	0.3982	0.3486
Standard deviation	0.00240	0.00303	0.0091	0.1042	0.0142	0.0377	0.0256	0.0261
No. of measured ratios N	74	74	74	74	74	74	74	74
s.e.m.	0.00028	0.00035	0.0011	0.0121	0.0017	0.0044	0.0030	0.0030
s.e.m. + bkg uncertainties[b]	0.00054	0.00073	0.0031	0.0668	0.0032	0.0089	0.0079	0.0125
δ wrt solar Xe [‰]	−13	−125	−101	1428	−64	−18	77	161
Error [‰]	111	174	37	64	20	11	21	42
ID#25269 (Static)	0.00464	0.00418	0.0746	2.5221	0.1537	0.8125	0.4026	0.3451
Standard deviation	0.00230	0.00252	0.0081	0.0888	0.0132	0.0351	0.0247	0.0215
No. of measured ratios N	198	198	198	198	198	198	198	198
s.e.m.	0.00016	0.00018	0.0006	0.0063	0.0009	0.0025	0.0018	0.0015
s.e.m. + bkg uncertainties[b]	0.00028	0.00048	0.0008	0.0063	0.0010	0.0030	0.0027	0.0023
δ wrt solar Xe [‰]	−51	−5	−114	1423.9	−67.4	−15.9	88.6	149.3
Error [‰]	58	115	10	6.5	6.2	4.0	7.5	7.8
Unweighted average	0.00473	0.00393	0.07514	2.5245	0.15396	0.8115	0.4004	0.3468
s.e.m.	0.00009	0.00025	0.00055	0.0024	0.00026	0.0010	0.0022	0.0017
δ wrt solar Xe [‰]	−32	−65	−108	1426.2	−65.8	−17.1	82.7	155.0
s.e.m. [‰]	23	62	7	3.3	2.3	1.9	6.2	6.0
$1/\sigma^2$-weighted average	0.00468	0.00403	0.07466	2.5221	0.15374	0.8123	0.4021	0.3452
Error	0.00025	0.00040	0.00077	0.0063	0.00094	0.0029	0.0026	0.0022
δ wrt solar Xe [‰]	−43	−41	−113	1424.0	−67.1	−16.2	87.4	149.7
Error [‰]	52	97	9	6.5	5.9	3.8	7.1	7.7
EETA 79001, Lith. C [1]	0.00378	0.00327	0.0735	2.394	0.1543	0.7930	0.4008	0.3514
Error	0.00022	0.00022	0.0011	0.029	0.0010	0.0077	0.0039	0.0036
EETA 79001, Zagami [2]	0.00353	0.00322	0.0724	2.384	0.1532	0.7934	0.3959	0.3475
Error	0.00040	≡ 0	0.0022	0.020	0.0010	0.0073	0.0042	0.0033
Genesis solar Xe [3]	0.00489	0.00420	0.08420	1.0405	0.16480	0.8256	0.36979	0.30030
Error	0.00006	0.00007	0.00020	0.0010	0.00030	0.0012	0.00059	0.00049
Solar fractionation factor [4]	0.7470	0.8035	0.8643	0.8964	0.9297	0.9642	1.0757	1.1570
Error[c]	0.0050	0.0040	0.0029	0.0022	0.0015	0.0008	0.0018	0.0038
Fractionated solar Xe	0.00365	0.00338	0.0728	0.9327	0.1532	0.7960	0.3978	0.3475
Error	0.00005	0.00006	0.0003	0.0025	0.0004	0.0013	0.0009	0.0013
Fract. solar wrt solar [‰]	−253	−196	−135.7	−103.6	−70.3	−35.8	75.7	157.0
Error [‰]	14	19	4.1	2.5	2.8	2.1	3.0	4.7

Table 2 References: [1] Swindle et al. (1986), [2] Mathew et al. (1998), [3] Meshik et al. (2015), [4] Appendix A6.
[a] $^{130}Xe/^{132}Xe$ ratios corrected for interference by ^{129}XeH hydride (Appendix A2). All ratio data in Appendix A7.
[b] Total error, including uncertainties in background (bkg) corrections. Error augmentations based on differences in isotope ratios yielded by the selected and alternate background subtraction models (Sec. 2.2).
[c] Estimated variance in fit to meteorite data.

nominal background model as described above and an alternate model. For Kr, the alternate background model used a tracer of m/z 55 in ID #25111 and m/z 63 in ID #25269. For Xe, the alternate background model for both ID #25253 and ID #25269 used a constant value at each relevant m/z, acquired before the Xe analysis region.

3. Results and discussion

The number N of individually measured and corrected isotope ratios, their standard deviation and standard error of their mean (s.e.m.), and assessment of total error are set out in Tables 2 and 3 for all Xe and Kr analyses. A total of ∼5000 individual ratios were included in the analyzed regions of the four experiments. Graphical displays of measurements vs. time, selected to include data sets for both low and high abundance Xe and Kr isotopes, are shown in Appendix A4. Tabulations of all Kr and Xe isotope ratio data used in the analyses, corrected for backgrounds, peak shapes and mass discriminations, are contained in Appendix A7.

The SAM isotopic compositions reported here for Xe and Kr in Mars' atmosphere are averages of results obtained in the repeated experiments, #25253 and #25269 for Xe and #25111 and #25269 for Kr. These were calculated in two ways from the separate experiment results: (a) unweighted averages with s.e.m. errors given by their standard deviation/$\sqrt{2}$; or (b) $1/\sigma_j^2$-weighted averages where σ_j is the ±1 sigma error in each of the two experiments. The first ignores errors in the individual experiment measurements, the second takes them explicitly into account. Final Xe and Kr compositions calculated using both averaging protocols are listed in Tables 2 and 3.

3.1. Xenon

Comparisons of the experiment ID#25253 and ID#25269 averages in Table 2 show satisfactory reproducibility of the separately measured isotopic compositions. Differences between the individual isotope ratio sets (e.g. $[^{124}Xe/^{132}Xe \pm \sigma]_{25269} - [^{124}Xe/^{132}Xe \pm \sigma]_{25253}$) are all <60% of the errors in the differences; across the Xe spectrum they average ∼30%. This agreement is reflected in the close correspondence of the unweighted and $1/\sigma^2$-weighted averages in Table 2, within—and for isotope masses >126 well within—their associated uncertainties. In this case it seems appropriate to select $1/\sigma^2$-weighted averaging: it biases results toward the more precise experiment #25269 data, and also generates more conservative errors than unweighted averaging.

Atmospheric Xe isotope ratios relative to ^{132}Xe generated from the SAM data in this way are plotted in Fig. 1 relative to the composition of Genesis SW-Xe (Meshik et al., 2015), together with measurements listed in Table 2 on shergottite glasses from EETA79001 (Swindle et al., 1986) and EETA79001 + Zagami (Mathew et al., 1998). Error bars are shown where they exceed the symbol sizes. Effects of adopting unweighted instead of

Table 3
Krypton.

	80/84	82/84	83/84	86/84
ID#25111 (Semi-static)	0.0666	0.2209	0.2021	0.3129
Standard deviation	0.0316	0.0598	0.0521	0.0651
No. of measured ratios *N*	247	247	247	247
s.e.m.	0.0020	0.0038	0.0033	0.0041
s.e.m. + bkg uncertainties[a]	0.0021	0.0041	0.0033	0.0042
δ wrt solar Kr [‰]	617	75	−6	39
Error [‰]	52	20	16	14
ID#25269 (Semi-static)	0.0779	0.2116	0.2025	0.2989
Standard deviation	0.0418	0.0657	0.0658	0.0810
No. of measured ratios N	432	432	432	432
s.e.m.	0.0020	0.0032	0.0032	0.0039
s.e.m. + bkg uncertainties[a]	0.0053	0.0080	0.0041	0.0057
δ wrt solar Kr [‰]	891	30	−4	−8
Error [‰]	129	39	20	19
Unweighted average	0.0723	0.2163	0.2023	0.3059
s.e.m.	0.0056	0.0047	0.0002	0.0070
δ wrt solar Kr [‰]	754	53	−5.4	16
s.e.m. [‰]	137	23	1.4[b]	23
$1/\sigma^2$-weighted average	0.0681	0.2190	0.2023	0.3075
Error	0.0020	0.0036	0.0026	0.0033
δ wrt solar Kr [‰]	654	66	−6	21
Error [‰]	48	18	13	11
EETA 79001, Lith. C [1]	0.0432	0.2063	0.2029	0.3009
Error	0.0007	0.0017	0.0015	0.0023
EETA 79001, Lith. C [2]	0.0440	0.2065	0.2044	0.2993
Error	0.0015	0.0028	0.0038	0.0039
Genesis solar Kr [3]	0.0412	0.2054	0.2034	0.3012
Error	0.0002	0.0002	0.0002	0.0004

Table 3 References: [1] Swindle et al. (1986), [2] Becker & Pepin, (1984), [3] Meshik et al. (2014).

[a] Total error, including uncertainties in background (bkg) corrections. Error augmentations based on differences in isotope ratios yielded by the selected and alternate background subtraction models (Sec. 2.2). Standard deviation and s.e.m. = standard deviation/$\sqrt{N}$ calculated using all individual ratios measured throughout the analysis region (Appendix A7).

[b] Small error likely fortuitous. Average expt. ID measurement error of $\sim \pm 18$‰ adopted for Fig. 2.

$1/\sigma^2$-weighted averaging are indicated by the white squares at ^{124}Xe and ^{126}Xe. The two averaging protocols yield statistically indistinguishable results at these minor isotopes, and in fact for all isotopes.

The solid curve in Fig. 1 represents Meshik et al.'s SW-Xe mass-fractionated in hydrodynamic escape (Appendix A6) to the degree required for best fit the EETA79001 and EETA + Zagami measurements. Correspondence of the curve with the meteorite data is striking. The SAM atmospheric measurements for isotopes heavier than ^{126}Xe generally follow the same pattern. Averaged δ^{128}Xe and δ^{130}Xe–δ^{136}Xe ratios in Fig. 1 agree with the fractionation curve, and therefore with the meteorites, to within ~25‰ or less. These direct *in situ* measurements support the conclusion from the meteorite data that the base composition of atmospheric Xe on Mars, except for the large radiogenic ^{129}Xe contribution, is fractionated solar Xe (Pepin, 2000). This conclusion is reinforced by the observation that Mars' interior (i.e., mantle) Xe is very similar to SW-Xe (Jakosky and Jones, 1997; Swindle and Jones, 1997; Ott, 1988; Swindle, 2002).

However significant offsets of the nonradiogenic atmospheric ratios from the curve are evident, large for δ^{124}Xe and δ^{126}Xe, smaller for δ^{128}Xe and δ^{131}Xe but still up to > 5x their mean errors above the average meteorite ratios. The origins of these nonradiogenic excesses are presently not understood. There are no identified analytic mass interferences at these isotopes that could account for them, from products found in SAM that could be contaminants in the gas processing manifold or mass spectrometer. We have calculated the potential effect of masses that could be associated with the degradation of the SAM derivatization reagent N-Methyl-N-(tert-butyldimethylsilyl)-trifluoroacetamide (MTBSTFA), vapors of which were previously reported to have been released and detected as a hydrocarbon background in SAM solid sample analyses (Glavin et al., 2013) and find that such a background subtraction would still be insufficient to account for the elevated ^{124}Xe and ^{126}Xe (Appendix A3). However small background signals are indeed seen at these masses, whatever their origin. These were incorporated into the background model and subtracted to yield corrected isotope ratios. It is interesting to note that Viking also detected high abundances at the trace masses 124 and 126, though they were unable to report them quantitatively (Owen et al., 1977). Although attributed to hydrocarbon contamination, they could alternatively suggest the interesting possibility that these, in part, were the first hint of elevated light masses of Xe in the martian atmosphere.

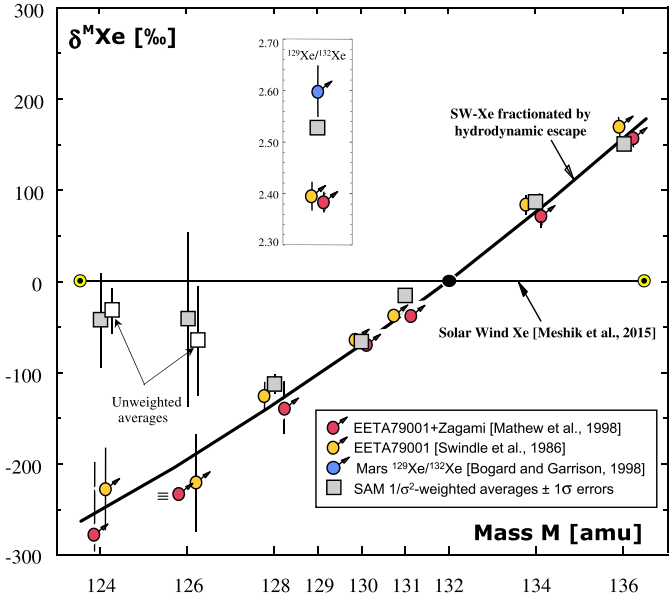

Fig. 1. Martian meteorite, fractionated solar wind, and average SAM Xe data plotted as δ-values referenced to the solar wind (SW) composition, where $\delta^{M}Xe = 1000[(^{M}Xe/^{132}Xe)_{measured}/(^{M}Xe/^{132}Xe)_{SW} - 1]$‰. SW ratios from Meshik et al. (2015). SAM ratios are $1/\sigma_j^2$-weighted averages of the two expt ID Xe averages in Table 2, where σ_j is the $\pm 1\sigma$ error in each (Sec. 3.1); $1/\sigma^2$-weighted error bars shown where exceeding symbol sizes. White squares at ^{124}Xe and ^{126}Xe are δ-values obtained by unweighted averaging of the two average expt ID ratios (Table 2). Differences between the heavier isotope δ-values for the two types of averaging are too small to be visible at the scale of the figure.

Another possible explanation for elevation of the light Xe isotope ratios above the SW fractionation curve, discussed in Sec. 3.3.1, is the presence of spallogenic and neutron-capture Xe produced by galactic cosmic ray (GCR) irradiation of target elements in soil and rocks on or near the martian surface and released over time into the atmosphere. Such degassing of a regolith product generated from neutron-irradiated Br is a likely explanation for the presence of excess ^{80,82}Kr in the atmospheric Kr trapped in the shergottite glasses (Sec. 3.2).

3.2. Krypton

SAM measurements at $m/z = 78$ were compromised by a large unresolved interference, most likely due to known benzene or dichloropropane fragmentation contaminants in the gas processing system. ^{78}Kr/^{84}Kr ratios are therefore not reported. Some of the other isotope ratios measured in the two Kr experiments show more scatter than is present in the Xe experiments. For ^{80}Kr/^{84}Kr and ^{86}Kr/^{84}Kr in particular, differences in ratio averages exceed

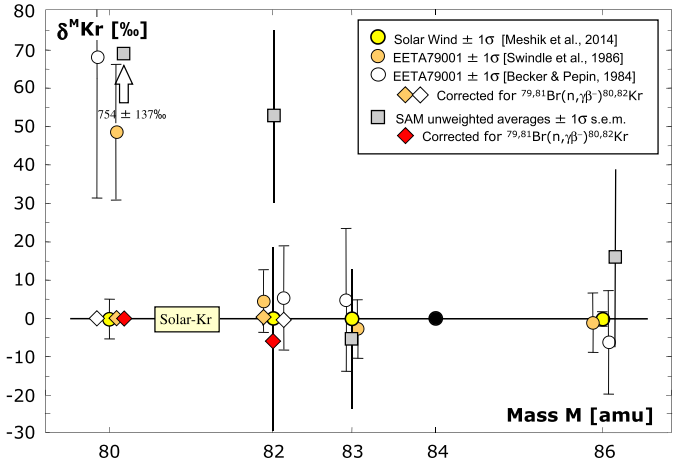

Fig. 2. Martian meteorite and average SAM Kr data plotted as δ-values referenced to the SW composition, where δ^{M}Kr is defined as in Fig. 1 with Kr isotope ratios replacing Xe ratios in the δ equation. SW ratios from Meshik et al. (2014). SAM ratios from the unweighted averages of the two Kr averages in Table 3. Error bars for the SAM data reflect $\pm 1\sigma$ standard errors of the means (s.e.m.) of the two data sets, except at ^{83}Kr where a more conservative error estimate is shown (Sec. 3.2, Table 3). Diamond symbols at M = 80 and 82 denote subtractions from measured ^{80,82}Kr/^{84}Kr ratios of isotopes produced by neutron capture in Br; details discussed in Sec. 3.2.

the errors in their differences by a factor of ~2 (Table 3). It is possible that dissimilar experimental techniques, including different gas pathways and scanning sequences for experiments #25111 and #25269, could have played a role. Modification of the method for Kr isotope measurements in #25269 was necessary in order to achieve the static mode for Xe isotope measurements, although the Kr was measured in semi-static mode (sec. 2.1). There is no evidence, however, that either of these analyses by itself is the better representative of atmospheric Kr composition. In this situation unweighted averaging of the data sets is the more conservative choice since the s.e.m. values overlap both of the individual experiment ID averages while errors associated with $1/\sigma^2$-weighted averages do not (Table 3). However, the uncertainty shown in the table for averaged ^{83}Kr/^{84}Kr is unrealistically small ($\sim \pm 1.5$‰) compared to other isotopes. It likely reflects fortuitous agreement of this ratio in the two experiments. An alternative and perhaps overly conservative estimate is the average uncertainty of $\sim \pm 18$‰ in the separate experiment measurements (Table 3).

Fig. 2 shows the averaged data from the SAM experiments compared to the solar wind (Meshik et al., 2014) and meteorite compositions. The SAM Kr isotopic distribution agrees with the SW composition within $\pm 1\sigma$ uncertainty at ^{86}Kr, and also at ^{83}Kr if the plotted alternate error suggested above is adopted, but show substantial enrichments above the SW trend for the light isotopes ^{80}Kr and ^{82}Kr. Elevations above SW-Kr at these two isotopes, although at considerably lower levels, are also observed in Kr trapped in shock glasses from the EETA79001 shergottite (Fig. 2) and are thought to result from neutron capture in Br via ^{79,81}Br$(n,\gamma\beta^-)^{80,82}$Kr (Becker and Pepin, 1984; Swindle et al., 1986; Rao et al., 2002). Moreover, there is evidence that these excesses originated on Mars, and are not due to capture of neutrons generated by in-space GCR irradiation during meteorite transits from Mars to Earth (Swindle et al., 1986; Rao et al., 2002).

The relative magnitudes of the ^{80,82}Kr excesses measured by SAM support the capture hypothesis. If the ^{80}Kr elevations are due solely to ^{79}Br$(n,\gamma\beta^-)^{80}$Kr reactions, one can calculate from the ^{79}Br and ^{81}Br neutron capture cross sections what the corresponding enhancement at ^{82}Kr from ^{81}Br$(n,\beta^-)^{82}$Kr would be. Sums of resonance integrals for high, epithermal, and thermal energy neutron capture in ^{79,81}Br (Dorval et al., 2008) yield an ^{80}Kr/^{82}Kr production ratio of 2.58 ± 0.25, indistinguishable from the ~2.5 ratio that accounts for ^{80}Kr and ^{82}Kr excesses in large chondritic meteorites (Marti et al., 1966). Application of Dorval et al.'s production ratio to the excesses above solar of ^{80,82}Kr observed in both the SAM and meteorite data (Table 3, Fig. 2) yields the corrected ^{80,82}Kr/^{84}Kr ratios indicated by the diamond symbols in Fig. 2. Corrected ^{80}Kr/^{84}Kr is solar ($\delta = 0$) by assumption. The n-corrected SAM ^{82}Kr/^{84}Kr ratio falls at $\delta = -6$‰, a nominal reduction of ~60‰ from the measured value. The attached error bar includes the ^{82}Kr/^{84}Kr measurement error plus augmentations due to uncertainties in measured ^{80}Kr/^{84}Kr and the ^{80}Kr/^{82}Kr production ratio.

It is evident that the ^{82}Kr/^{84}Kr ratios, without their n-capture components, are close to solar for both the meteorite measurements and those reported here for the atmosphere if the corrected ^{80}Kr/^{84}Kr ratios are likewise solar. This strengthens the view that Mars' base atmospheric Kr composition is in fact solar, overlain by neutron capture components at ^{80,82}Kr. An unexplained puzzle is why the meteorite glasses, which purport to sample the recent atmosphere, display much smaller n-capture excesses than those in the present-day atmosphere (Fig. 2).

Garrison and Bogard (1998) propose that enrichments of $^{80-83}$Kr/^{84}Kr and a depletion of ^{86}Kr/^{84}Kr relative to the solar composition, observed in one sample of EETA 79001 impact glass, signal the presence of mass-fractionated solar Kr in which an ^{80}Kr excess is absent or minor. However, both the meteorite and direct atmospheric measurements in Fig. 2, including those of Swindle et al. (1986) which are viewed as the most precise for the meteorites, show no evidence for such fractionation.

3.3. Regolith-derived spallation and neutron-capture Xe and Kr in the martian atmosphere?

3.3.1. Xenon

Excesses in δ^{124}Xe and δ^{126}Xe are often signatures of spallation Xe components. Their presence in the SAM data suggests that the martian atmosphere may contain spallogenic and neutron capture products generated in and outgassed from the regolith (Rao et al., 2002). Assuming that atmospheric spallation and $(n,\gamma\beta^-)$ components are actually present in the atmosphere, corrections to the SAM measurements were calculated using the following parameters:

3.3.1.1. A REE/Ba wt.% ratio of 0.54 GCR spallations of Ba and the rare earth elements (REE) are the dominant contributors to spallogenic Xe. Spallation Xe production rates for these elements are given in Hohenberg et al. (1978). They are calculated using a ratio of 6.9 for REE abundances summed from Ce to Er, relative to La abundance. Of interest for this model is Hohenberg et al.'s (Ce + Pr)/La ratio of 3.0. In the 6 SNC meteorites for which data exist in the Lodders (1998) compilation, this ratio is 3.0 ± 0.5. Although there are insufficient SNC abundance data to enable similar comparisons for most of the heavier REEs, this agreement suggests that they are also likely to be approximately compatible with Hohenberg et al.'s REE distributions. The SNC La/Ba ratio is $0.069 \pm 10\%$ (Lodders, 1998), and therefore "La"/Ba, with "La" including all the REE targets, is probably reasonably close to $0.069 \times (1 + 6.9) = 0.54$. REE concentrations on Mars are unknown. The REE/Ba ratio of 0.54 that arguably characterizes the SNC meteorites is taken as proxy for the martian regolith.

Spallation production rates used in this modeling are from Hohenberg et al. (1978), calculated for a La/Ba ratio set to 0.069 and an adjustable Ba abundance (Sec. 3.3.1.3). They are integrated over a regolith depth of ~500 g/cm^2. The resulting spallation composition is listed in Table 4. To account for the present atmospheric overburden of ~17 g/cm^2 the regolith surface was repositioned to 17 g/cm^2 and production rates were integrated from this depth to

Table 4
ID#25269 xenon corrected for spallation and $(n, \gamma\beta^-)$ products.

	124/132	126/132	128/132	129/132	130/132	131/132	134/132	136/132
Measured (Table 3)	0.00464	0.00418	0.07459	2.5221	0.15369	0.8125	0.4026	0.3451
Total error[a]	0.00028	0.00048	0.00080	0.0063	0.00098	0.0031	0.0027	0.0023
δ wrt solar Xe [‰]	−51	−5	−114	1423.9	−67.4	−15.9	88.6	149.3
Error [‰]	58	115	10	6.5	6.2	4.0	7.5	7.8
Spallation composition[b]	0.609	≡ 1	1.509	1.765	0.662	3.19	0.031	0
Error	0.007		0.023	0.043	0.014	0.15	0.001	
Measured minus spallation	0.00395	0.00310	0.07277	2.5221	0.15293	0.8090	0.4026	0.3451
Δ wrt measured Xe	−0.00069	−0.00108	−0.00183	0	−0.00076	−0.0035	0	0
Δ/measured Xe [‰]	−149	−258	−24.4	0	−4.9	−4.3	0	0
Measured minus $(n, \gamma\beta^-)$[c]	0.00464	0.00418	0.07451	2.5221	0.15369	0.7916	0.4026	0.3451
Δ wrt measured Xe	0	0	−0.00008	0	0	−0.0209	0	0
Δ range wrt measured Xe			∼0			−0.0163		
			−0.00081			−0.0753		
Δ/measured Xe [‰]	0	0	−1.1	0	0	−26	0	0
Δ range/measured Xe [‰]			0/−10.9			+20/−93		
Corrected ID#25269	0.00395	0.00310	0.07269	2.5221	0.15293	0.7882	0.4026	0.3451
± uncertainty	0.00028	0.00048	+0.00080	0.0063	0.00098	+0.0166	0.0027	0.0023
			−0.00108			−0.0754		
δ wrt solar Xe [‰]	−192	−262	−136.7	1424.0	−72.0	−45.3	88.6	149.3
± uncertainty [‰]	58	115	+9.8	6.5	6.2	+20.2	7.5	7.8
			−13.0			−91.3		
δ wrt fract. solar Xe [‰]	81	−81	−1.1	1704	−1.8	−9.9	12.0	−6.7
Uncertainty [‰]	78	143	+11.8	10	6.9	+20.9	7.2	7.5
			−15.4			−94.7		
Fract. solar wrt solar [‰]	−253	−196	−135.7	−103.6	−70.3	−35.8	75.7	157.0
Uncertainty [‰]	14	19	4.1	2.5	2.8	2.1	3.0	4.7

[a] See Table 2, footnote (b).
[b] Spallation $^{132}Xe/^{126}Xe = 0.504 \pm 0.013$. Degassed spallogenic contributions to atmospheric ^{132}Xe and ^{129}Xe inventories are negligible, 0.5‰ and 0.7‰ respectively. Neither of these is included in spallation corrections to measured $^{M}Xe/^{132}Xe$ ratios.
[c] For $^{127}I(n, \gamma\beta^-)^{128}Xe$, $^{127}I = 100$ ppb ± a factor 10. For $^{130}Ba(n, \gamma\beta^-)^{131}Xe$ and Ba = 602 ppm, adopted ^{131}Xe production rate (PR) = log average of the Hohenberg et al. (1978) and Rao et al. (2002) PRs. Upper and lower Δ ranges calculated for each of these PRs separately.

500 g/cm^2. No attempt was made to calculate production rate variations due to different—and unknown—atmospheric densities that could have occurred over the past 3700 Ma.

3.3.1.2. A 43% regolith degassing efficiency Martian Br is taken to be 36 ppm, about midway in the concentration range measured by Pathfinder (Gellert et al., 2004) and Curiosity (Blake et al., 2013). Combined with modeling of neutron capture by ^{79}Br in the regolith (Rao et al., 2002) the ^{80}Kr excess measured by SAM (Fig. 2) requires 43% degassing of the regolith inventory produced over 3700 Ma by GCR-generated neutrons. This 43% release is assumed to apply to spallogenic and $(n, \gamma\beta^-)$ Xe products as well.

3.3.1.3. With these choices, the Ba concentration in the martian regolith is a free parameter in the model Results of applying it to the static experiment #25269 Xe measurements, the more precise of the two data sets, are shown in Fig. 3. Barium abundance was adjusted until spallation-corrected $\delta^{124}Xe$ and $\delta^{126}Xe$ were equally spaced on either side of the fractionated SW curve, both within $\sim 1\sigma$ error of the curve or less (Fig. 4). Required Ba concentration in this baseline model is 602 ppm. Other fits of corrected $\delta^{124}Xe$ and $\delta^{126}Xe$ to fractionated SW are possible; for example, error-weighting their positions relative to the curve, which would move $\delta^{124}Xe$ closer and $\delta^{126}Xe$ further away. But this has only a minor (<10%) effect on required Ba.

Effects on isotope ratios of subtracting calculated spallation and neutron capture components are set out numerically in Table 4 and plotted in Fig. 3 and, at higher resolution, in Fig. 4. Essentially all of the $\delta^{128}Xe$ excess is removed by spallation correction. Additional production of ^{128}Xe by $^{127}I(n, \gamma\beta^-)^{128}Xe$ capture is probably minor. Estimates for iodine in the martian regolith range from ∼100 ppb in three non-Antarctic, presumably uncontaminated SNCs (Lodders, 1998) to ∼500 ppb with large uncertainty

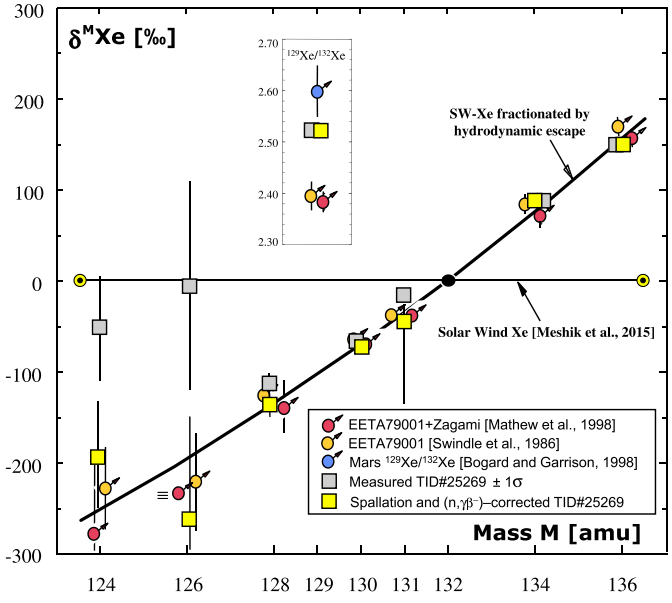

Fig. 3. As in Fig. 1, but here for measured SAM Xe ratios and errors in expt ID #25269 alone. Corrections for hypothetical atmospheric spallation and n-capture $^{127}I(n, \gamma\beta^-)^{128}Xe$ and $^{130}Ba(n, \gamma\beta^-)^{131}Xe$ components (yellow squares) discussed in Sec. 3.3 and listed in Table 4. Upper and lower tips of the asymmetric error bar around $\delta^{131}Xe$ denote different corrections calculated for $^{130}Ba(n, \gamma\beta^-)^{131}Xe$ contributions using, respectively, the Hohenberg et al. (1978) and Rao et al. (2002) n-capture production rates.

(Rao et al., 2002). Correction for production from iodine at the 100 ppb level is negligible (∼1‰), and only ∼10‰ even with 10x this abundance (Table 4). Spallation corrections to measured

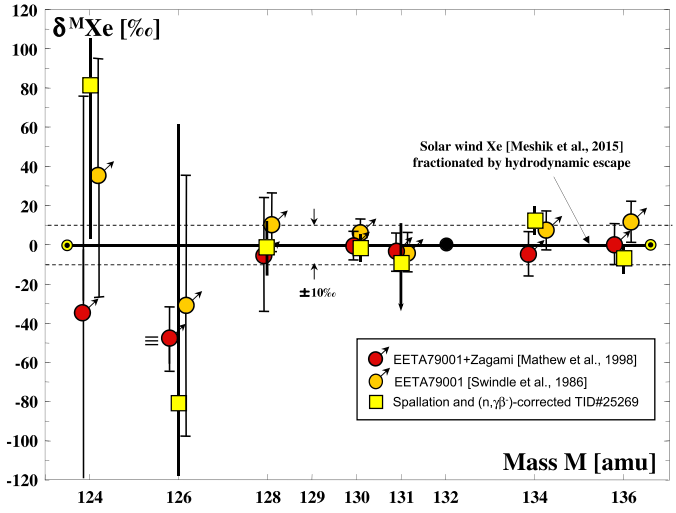

Fig. 4. expt ID #25269 Xe ratios corrected for spallation and $(n, \gamma\beta^-)$ products (yellow squares) compared with fractionated solar Xe ratios. The expt ID #25269 and meteorite data are referenced here to the fractionated solar composition itself and differences are therefore illustrated at higher resolution than in Fig. 3. Discussion and data in Sec. 3.3.1 and Table 4. See Fig. 3 caption for discussion of asymmetric error at δ^{131}Xe.

δ^{130}Xe and δ^{131}Xe are small (<5‰). Most of the δ^{131}Xe excess is attributable to n-capture in Ba, but the ^{130}Ba$(n, \gamma\beta^-)^{131}$Xe contribution is uncertain because the production rates given by Rao et al. (2002) and estimated from Hohenberg et al. (1978) differ by a factor of ∼20, due primarily to a ∼6-fold difference in adopted capture cross sections. Using the log average of the two ^{130}Ba$(n, \gamma\beta^-)^{131}$Xe production rates—1.9×10^{15} atoms/s for Ba = 602 ppm in the baseline model—corrects δ^{131}Xe to within 10‰ of the fractionation curve, but with the large uncertainties shown in Table 4 and Fig. 3. Other isotope ratios (δ^{134}Xe, δ^{136}Xe, and ^{129}Xe/^{132}Xe) are essentially unchanged by spallation subtraction. Fig. 4 demonstrates that correction of the measured ID #25269 isotope ratios for the assumed presence of atmospheric spallation and $(n, \gamma\beta^-)$ products leads to notable agreement with the fractionated SW and shergottite glass compositions. All corrected isotope ratios fall within error in the ±10‰ band around the fractionated SW reference composition, and only δ^{134}Xe is $>1\sigma$ away from the reference.

The 602 ppm Ba content obtained for the baseline model is sensitive to adopted values of a number of parameters: (a) the ^{132}Xe atmospheric volume mixing ratio (VMR), not measured directly by SAM (Sec. 2.1) but derived from the measured ^{36}Ar VMR in Mars' atmosphere (Atreya et al., 2013; Mahaffy et al., 2013) and an estimate of ^{132}Xe/^{36}Ar from the shergottite glasses (Garrison and Bogard, 1998); (b) the La/Ba ratio in the martian regolith (Sec. 3.3.1.1); and (c) the regolith Br abundance which sets the regolith outgassing efficiency (Sec. 3.3.1.2). The latter has the most severe impact on Ba requirements. As regolith Br is varied over its most likely range of ∼20–60 ppm (Blake et al., 2013; Gellert et al., 2004) with corresponding changes in regolith degassing efficiencies from 76% to 26% respectively, the Ba concentrations needed to replicate Figs. 3 and 4 range from 340 to 1020 ppm. Variations in any of these parameters produce proportional changes in required Ba, and so one cannot specify a single regolith Ba content that uniquely generates Figs. 3 and 4. However the model is resilient to parameter variations in the sense that a particular Ba value can always be found that reproduces the corrected composition in the figures. Varying these parameters within their probable uncertainty ranges leads to a spread in required Ba of ∼200 to 1000 ppm.

3.3.1.4. Barium Barium in martian soils and rocks has been measured by Curiosity's ChemCam LIBS instrument. Estimates range from a few 10's of ppm in sand and soil up to ∼1640 ppm in a trachyte rock (Ollila et al., 2014; Payré et al., 2016); the majority of the measurements fall between ∼100 and 500 ppm (Payré et al., 2016). The Ba concentration of ∼600 ppm in the baseline spallation model is significantly above their average. However, the ∼200–1000 ppm spread in required Ba concentrations generated by variations in modeling parameters falls with the range of LIBS measurements reported by Payré et al.

Within its uncertainties, the Ba content of the martian regolith required by the model may be compared to the ∼250 ppm estimate for Earth's bulk crust (McLennan, 2001; Payré et al., 2016) and ∼350 ppm in ocean island basalts (OIB) (Sun and McDonough, 1989). The REE/Ba ratio of 0.54 adopted for Mars is close to Sun and McDonough's OIB value of ∼0.56 and intermediate between ∼0.34 in Earth's bulk continental crust (McLennan, 2001) and ∼1.2 in oceanic crust (White and Klein, 2014), consistent with the more mafic nature of the martian surface compared to the terrestrial continental crust.

3.3.1.5. Comparison with Xe trapped in shergottite glasses This spallation scenario is potentially capable of accounting for observed excesses in the SAM Xe data at nonradiogenic isotopes lighter than ^{132}Xe. It conflicts, however, with evidence that shock glasses in shergottites record the composition of the martian atmosphere. Xe trapped in glassy phases of EETA79001 (Swindle et al., 1986) and EETA79001 + Zagami (Mathew et al., 1998), plotted in Fig. 1, shows no evidence for the presence of atmospheric spallation or neutron capture Xe. These meteorites do display spallogenic enrichments in the light Xe isotopes, particularly in Zagami with its long exposure age, but these are consistent with production in space by GCR spallation during post-ejection transit from Mars to Earth (Swindle et al., 1986; Mathew et al., 1998). When these in situ spallation products are subtracted, δ^{124}Xe, δ^{126}Xe, and δ^{128}Xe ratios in the glasses fall close to the SW fractionation curve (Fig. 1) with no evident way to accommodate additional atmospheric spallation or $(n, \gamma\beta^-)$ components.

This could be a telling argument against the spallation hypothesis if the light isotope enhancements recorded by SAM could be shown to be attributable to hydrocarbon interferences, but no plausible candidates among species known to be present in the QMS analytic system have been identified (Appendix A3.1). The alternative to instrumental interferences, where the SAM light isotope signatures are taken to be true measures of atmospheric composition, would seem to require a specific degassing history for the martian regolith in which the bulk of spallation Xe products was released after the shergottite glasses had acquired their trapped atmosphere. However, there is relatively strong evidence that ^{80,82}Kr from neutron capture in regolith Br *was* degassed to the atmosphere and incorporated into the glasses (Sec. 3.2). At the moment neither of these potential explanations, either SAM hydrocarbon interferences or an arbitrarily constructed spallation degassing scenario, is particularly robust.

3.3.2. Atmospheric fission Xe on Mars?

Mars' atmosphere is notable for the large ^{129}Xe excess displayed by the SAM and shergottite glass measurements in Figs. 1 and 3, yet in none of these data sets are there discernable elevations of heavy isotope ratios that would signal the existence of a ^{244}Pu fission Xe component expected to accompany outgassed radiogenic ^{129}Xe (Swindle and Jones, 1997). Models suggesting that Pu–Xe is actually present but concealed, and their status from the perspective of the meteorite and SAM data in Tables 2 and 4, are discussed in Appendix A5.

3.3.3. Krypton

The elevated atmospheric $^{80,82}Kr/^{84}Kr$ ratios measured by SAM (Sec. 3.2) appear to be consistent with addition of a Kr component generated in the regolith by neutron capture in Br. One would expect that release of these products into the atmosphere would be accompanied by degassing of Kr produced by GCR spallation of Rb, Sr, and other target elements. However, unlike the case for the light Xe isotopes, addition of spallogenic Kr has only a minimal and undetectable effect on measured Kr isotopic abundances. Average regolith Rb (65 ppm) and Sr (225 ppm) concentrations are reported by Payré et al. (2016) and estimates of Y/Sr (∼0.74) and Zr/Sr (∼0.37) by Clark et al. (1976). Using elemental production rates from these elements (Hohenberg et al., 1978) and the 43% degassing efficiency of regolith inventories required by the SAM ^{80}Kr excess and the selected martian Br concentration of 36 ppm (Sec. 3.3.1.2), calculated spallation contributions elevate ^{80}Kr by only ∼2‰ and by <1‰ at the heavier isotopes.

4. Conclusions

SAM measurements of martian atmospheric Kr and Xe provide an in-situ benchmark for the SNC meteorite values. We see enrichments above the SNC isotopic values, particularly in the lighter isotopes of both Kr and Xe. What remains unclear, in particular for Xe, are the source(s) of the excesses. Either analytic mass interferences or the presence of atmospheric spallation and neutron capture components could cause such effects in Xe. The first of these possibilities seems doubtful since interfering species of sufficient magnitude appear to be absent in the SAM analytic system. The second is capable of explaining Xe isotope excesses relative to the fractionated SW composition, but conflicts with the observation that such components are not recorded in atmospheric Xe trapped in the shergottite glassy phases.

The elevated light isotopes in Kr (Fig. 2) are consistent with neutron capture in regolith bromine. The SAM measurements lend support to the proposal that Kr (and Xe) from neutron capture has been produced in the regolith and released into the atmosphere over time (Rao et al., 2002).

Measured $\delta^{134}Xe$ and $\delta^{136}Xe$ values are subject to neither resolvable spallation corrections or plausible mass interferences. SAM averages at these isotopes, and at $\delta^{130}Xe$ where a spallation contribution is minor, differ from the corresponding meteorite averages by <12‰ (Fig. 1). This strongly suggests that the base composition of Mars' atmospheric Xe follows the SW fractionation curve defined by the meteorite data. An assumed presence of spallation and $(n, \gamma\beta^-)$ Xe in the atmosphere can quantitatively account for elevations above the curve for the remaining nonradiogenic isotopes (Fig. 4).

The new SAM Xe data reinforce an old and enigmatic problem related to martian actinide chemistry and degassing history. Decay products of the extinct radionuclides ^{129}I and ^{244}Pu are both present in Earth's atmosphere (Pepin, 2000), but on Mars only one of these, a large excess of radiogenic ^{129}Xe, is apparent. This mystery has driven modeling attempts to argue that Xe from fission of ^{244}Pu actually is present in Mars' atmosphere but is fortuitously concealed from observation. Evaluation of such models in the context of the SAM and meteorite Xe data reported here suggests they are only marginally viable and in any case allow at most a minor contribution of Pu–Xe to the atmosphere (Appendix A5). Its near absence likely points to a very specific outgassing history for Mars, one in which ^{129}Xe from short-lived ^{129}I was released in early degassing but fission Xe from longer-lived ^{244}Pu is still sequestered within the planet.

It appears from the SAM Xe and Kr measurements that plausible arguments can be made for the presence of spallation and neutron capture products in the contemporary martian atmosphere. There are implications in this observation for understanding the breadth of regolith degassing by impact and other thermal pulses, and perhaps for the age of trapped atmosphere components in martian meteorites on the basis of accumulating *n*-capture and spallogenic contributions to the krypton and xenon inventories.

Acknowledgements

Special thanks to Richard Becker for helpful discussion regarding the data analysis. We are indebted to G. Avice and two anonymous reviewers for comments that greatly improved the manuscript. This work was funded by NASA's Mars Science Laboratory mission.

Appendix A. Supplementary material

Supplementary material related to this article can be found online at http://dx.doi.org/10.1016/j.epsl.2016.08.028.

References

Agee, C.B., Wilson, N.V., McCubbin, F.M., Ziegler, K., Polyak, V.J., Sharp, Z.D., Asmerom, Y., Nunn, M.H., Shaheen, R., Thiemens, M.H., 2013. Unique meteorite from early Amazonian Mars: water-rich basaltic breccia Northwest Africa 7034. Science 339, 780–785.

Atreya, S.K., Trainer, M.G., Franz, H.B., Wong, M.H., Manning, H.L., Malespin, C.A., Mahaffy, P.R., Conrad, P.G., Brunner, A.E., Leshin, L.A., 2013. Primordial argon isotope fractionation in the atmosphere of Mars measured by the SAM instrument on Curiosity and implications for atmospheric loss. Geophys. Res. Lett. 40, 5605–5609.

Becker, R.H., Pepin, R.O., 1984. The case for a Martian origin of the shergottites: nitrogen and noble gases in EETA 79001. Earth Planet. Sci. Lett. 69, 225–242.

Blake, D.F., Morris, R., Kocurek, G., Morrison, S., Downs, R., Bish, D., Ming, D., Edgett, K., Rubin, D., Goetz, W., 2013. Curiosity at Gale crater, Mars: characterization and analysis of the Rocknest sand shadow. Science 341, 1239505.

Bogard, D.D., Garrison, D.H., 1998. Relative abundances of argon, krypton, and xenon in the Martian atmosphere as measured in Martian meteorites. Geochim. Cosmochim. Acta 62, 1829–1835.

Bogard, D.D., Johnson, P., 1983. Martian gases in an Antarctic meteorite? Science 221, 651–654.

Cartwright, J., Ott, U., Herrmann, S., Agee, C., 2014. Modern atmospheric signatures in 4.4 Ga Martian meteorite NWA 7034. Earth Planet. Sci. Lett. 400, 77–87.

Clark, B.C., Baird, A., Rose, H.J., Toulmin, P., Keil, K., Castro, A.J., Kelliher, W.C., Rowe, C.D., Evans, P.H., 1976. Inorganic analyses of Martian surface samples at the Viking landing sites. Science 194, 1283–1288.

Dorval, E.L., Arribére, M.A., Guevara, S.R., 2008. Measurement of neutron capture resonance integrals on bromine isotopes. Nucl. Sci. Eng. 159, 199–212.

Franz, H.B., Trainer, M.G., Wong, M.H., Manning, H.L., Stern, J.C., Mahaffy, P.R., Atreya, S.K., Benna, M., Conrad, P.G., Harpold, D.N., Leshin, L.A., Moleskin, C.A., McKay, C.P., Nolan, J.T., Raaen, E., 2014. Analytical techniques for retrieval of atmospheric composition with the quadrupole mass spectrometer of the Sample Analysis at Mars instrument suite on Mars Science Laboratory. Planet. Space Sci. 96, 99–113.

Garrison, D.H., Bogard, D.D., 1998. Isotopic composition of trapped and cosmogenic noble gases in several Martian meteorites. Meteorit. Planet. Sci. 33, 721–736.

Gellert, R., Rieder, R., Anderson, R., Brückner, J., Clark, B., Dreibus, G., Economou, T., Klingelhöfer, G., Lugmair, G., Ming, D., 2004. Chemistry of rocks and soils in Gusev Crater from the alpha particle X-ray spectrometer. Science 305, 829–832.

Glavin, D.P., Freissinet, C., Miller, K.E., Eigenbrode, J.L., Brunner, A.E., Buch, A., Sutter, B., Archer, P.D., Atreya, S.K., Brinckerhoff, W.B., 2013. Evidence for perchlorates and the origin of chlorinated hydrocarbons detected by SAM at the Rocknest aeolian deposit in Gale Crater. J. Geophys. Res., Planets 118, 1955–1973.

Hohenberg, C., Podosek, F., Shirck, J., Marti, K., Reedy, R., 1978. Comparisons between observed and predicted cosmogenic noble gases in lunar samples. In: 9th Lunar and Planetary Science Conference Proceedings, pp. 2311–2344.

Jakosky, B.M., Jones, J.H., 1997. The history of Martian volatiles. Rev. Geophys. 35, 1–16.

Lodders, K., 1998. A survey of shergottite, nakhlite and chassigny meteorites whole-rock compositions. Meteorit. Planet. Sci. 33, A183–A190.

Mahaffy, P.R., Webster, C.R., Atreya, S.K., Franz, H., Wong, M., Conrad, P.G., Harpold, D., Jones, J.H., Leshin, L.A., Manning, H., 2013. Abundance and isotopic composition of gases in the martian atmosphere from the Curiosity rover. Science 341, 263–266.

Mahaffy, P.R., Webster, C.R., Cabane, M., Conrad, P.G., Coll, P., Atreya, S.K., Arvey, R., Barciniak, M., Benna, M., Bleacher, L., 2012. The sample analysis at Mars investigation and instrument suite. Space Sci. Rev. 170, 401–478.

Marti, K., Eberhardt, P., Geiss, J., 1966. Spallation, fission, and neutron capture anomalies in meteoritic krypton and xenon. Z. Naturforsch., A 21, 398–426.
Mathew, K.J., Kim, J.S., Marti, K., 1998. Martian atmospheric and indigenous components of xenon and nitrogen in SNC meteorites. Meteorit. Planet. Sci. 33, 655–664.
McLennan, S.M., 2001. Relationships between the trace element composition of sedimentary rocks and upper continental crust. Geochem. Geophys. Geosyst. 2.
Meshik, A., Hohenberg, C., Pravdivtseva, O., Burnett, D., 2014. Heavy noble gases in solar wind delivered by Genesis mission. Geochim. Cosmochim. Acta 127, 326–347.
Meshik, A., Pravdivtseva, O., Hohenberg, C., Burnett, D., 2015. Refined composition of solar wind xenon delivered by genesis: implication for primitive terrestrial xenon. In: 46th Lunar and Planetary Science Conference. Abstract #2640.
Mohapatra, R.K., Schwenzer, S.P., Herrmann, S., Murty, S., Ott, U., Gilmour, J.D., 2009. Noble gases and nitrogen in Martian meteorites Dar al Gani 476, Sayh al Uhaymir 005 and Lewis Cliff 88516: EFA and extra neon. Geochim. Cosmochim. Acta 73, 1505–1522.
Ollila, A.M., Newsom, H.E., Clark, B., Wiens, R.C., Cousin, A., Blank, J.G., Mangold, N., Sautter, V., Maurice, S., Clegg, S.M., 2014. Trace element geochemistry (Li, Ba, Sr, and Rb) using Curiosity's ChemCam: early results for Gale crater from Bradbury Landing Site to Rocknest. J. Geophys. Res., Planets 119, 255–285.
Ott, U., 1988. Noble gases in SNC meteorites: Shergotty, Nakhla, Chassigny. Geochim. Cosmochim. Acta 52, 1937–1948.
Owen, T., Biemann, K., 1976. Composition of the atmosphere at the surface of Mars: detection of argon-36 and preliminary analysis. Science 193, 801–803.
Owen, T., Biemann, K., Rushneck, D., Biller, J., Howarth, D., LaFleur, A., 1976. The atmosphere of Mars: detection of krypton and xenon. Science 194, 1293–1295.
Owen, T., Biemann, K., Rushneck, D., Biller, J., Howarth, D., Lafleur, A., 1977. The composition of the atmosphere at the surface of Mars. J. Geophys. Res. 82, 4635–4639.
Payré, V., Fabre, C., Cousin, A., Forni, O., Gasnault, O., Rapin, W., Meslin, P.Y., Sautter, V., Maurice, S., Wiens, R.C., Clegg, S., 2016. Trace elements in Gale Crater: Li, Sr, Rb and Ba abundances using ChemCam data. In: 47th Lunar and Planetary Science Conference. Abstract #1348.
Pepin, R.O., 1985. Evidence of Martian origins. Nature 317, 473–475.
Pepin, R.O., 1991. On the origin and early evolution of terrestrial planet atmospheres and meteoritic volatiles. Icarus 92, 2–79.
Pepin, R.O., 2000. On the isotopic composition of primordial xenon in terrestrial planet atmospheres. Space Sci. Rev. 92, 371–395.
Podosek, F.A., Ozima, M., 2000. The xenon age of the Earth. In: Origin of the Earth and Moon, vol. 1, pp. 63–72.
Rao, M., Bogard, D., Nyquist, L., McKay, D., Masarik, J., 2002. Neutron capture isotopes in the Martian regolith and implications for Martian atmospheric noble gases. Icarus 156, 352–372.
Schwenzer, S., Greenwood, R., Kelley, S., Ott, U., Tindle, A., Haubold, R., Herrmann, S., Gibson, J., Anand, M., Hammond, S., 2013. Quantifying noble gas contamination during terrestrial alteration in Martian meteorites from Antarctica. Meteorit. Planet. Sci. 48, 929–954.
Sun, S.-S., McDonough, W.F., 1989. Chemical and isotopic systematics of oceanic basalts: implications for mantle composition and processes. Geol. Soc. (Lond.) Spec. Publ., vol. 42, pp. 313–345.
Swindle, T.D., Caffee, M.W., Hohenberg, C.M., 1986. Xenon and other noble gases in shergottites. Geochim. Cosmochim. Acta 50, 1001–1015.
Swindle, T.D., Jones, J.H., 1997. The xenon isotopic composition of the primordial Martian atmosphere: contributions from solar and fission components. J. Geophys. Res., Planets 102, 1671–1678.
Swindle, T.D., 2002. Martian noble gases. Rev. Mineral. Geochem. 47, 171–190.
Treiman, A.H., 1998. The history of Allan Hills 84001 revised: multiple shock events. Meteorit. Planet. Sci. 33, 753–764.
Treiman, A.H., 2005. The nakhlite meteorites: augite-rich igneous rocks from Mars. Chem. Erde-Geochem. 65, 203–270.
Treiman, A.H., Dyar, M.D., McCanta, M., Noble, S.K., Pieters, C.M., 2007. Martian dunite NWA 2737: petrographic constraints on geological history, shock events, and olivine color. J. Geophys. Res., Planets 1991–2012, 112.
Treiman, A.H., Filiberto, J., 2015. Geochemical diversity of shergottite basalts: mixing and fractionation, and their relation to Mars surface basalts. Meteorit. Planet. Sci. 50, 632–648.
White, W.M., Klein, E.M., 2014. Composition of the oceanic crust. In: Treatise of Geochemistry, 2nd ed., pp. 457–496.
Wiens, R.C., Pepin, R.O., 1988. Laboratory shock emplacement of noble gases, nitrogen, and carbon dioxide into basalt, and implications for trapped gases in shergottite EETA 79001. Geochim. Cosmochim. Acta 52, 295–307.
Wiens, R.C., Becker, R.H., Pepin, R.O., 1986. The case for a Martian origin of the shergottites, II. Trapped and indigenous gas components in EETA 79001 glass. Earth Planet. Sci. Lett. 77, 149–158.